

CMB polarization map derived from the WMAP 5 year data through Harmonic Internal Linear Combination

Jaiseung Kim,^{*} Pavel Naselsky, and Per Rex Christensen
Niels Bohr Institute, Blegdamsvej 17, DK-2100 Copenhagen, Denmark
 (Dated: May 29, 2019)

We have derived whole-sky CMB polarization maps from the WMAP 5 year polarization data, using the Harmonic Internal Linear Combination (HILC) method. Our HILC method incorporates spatial variability of linear weights in a natural way and yields continuous linear weights over the entire sky. To estimate the power spectrum of HILC maps, we have derived a unbiased quadratic estimator, which is similar to the WMAP team's cross power estimator, but in a more convenient form for HILC maps. From our CMB polarization map, we have obtained TE correlation and E mode power spectra without applying any mask. They are similar to the WMAP team's estimation and consistent with the WMAP best-fit Λ CDM model. Foreground reduction by HILC method is more effective for high resolution and low noise data. Hence, our HILC method will enable effective foreground reduction in polarization data from the Planck surveyor.

PACS numbers: 98.70.Vc, 98.80.Es

I. INTRODUCTION

The Cosmic Microwave Background (CMB) is expected to be linearly polarized by Thompson scattering at the last scattering surface and after re-ionization. Most useful information on re-ionization and primordial gravitational wave can be obtained from CMB polarization on large angular scales [1, 2, 3, 4].

Foregrounds degrade the attainable accuracy of cosmological information [5] and particularly Galactic foregrounds are significant on large angular scales [6, 7]. Hence, the ability to clean foreground contamination without reliance to masking is of the utmost importance for the study of CMB polarization on large angular scales.

Recently, multi-frequency polarization data for the whole sky is available from the Wilkinson Microwave Anisotropy Probe (WMAP) [2, 8]. For cosmological analysis, the WMAP team used foreground-reduced maps obtained by a template fitting method. Due to heavy foreground contamination within their Galactic mask, the WMAP team's foreground-reduced polarization maps are not suitable for whole-sky CMB polarization maps. The WMAP team also produced a low resolution CMB polarization map by Markov Chain Monte Carlo (MCMC) method [9]. The MCMC map also contain heavy foreground contamination within the Galactic cut [9], which makes it unsuitable for whole-sky polarization maps. On the other hand, Internal Linear Combination (ILC) method is one of best blind approaches available in spite of a few drawbacks. Hence, several variants of ILC methods have been developed and implemented to construct a whole-sky CMB temperature map [10, 11, 12, 13, 14, 15]. Meanwhile, whole-sky CMB polarization maps are quite scarce at the moment. We have, from the WMAP 5 year polarization data, derived a whole-sky CMB polarization

map through the Harmonic Internal Linear Combination (HILC) method, which is natural extension of our previous effort to derive a CMB temperature map [13].

The outline of this paper is as follows. In Sec. II, we discuss Stokes parameters in the context of an all-sky analysis. In Sec. III, we discuss briefly foreground reduction method with multi-frequency maps. In Sec. IV, we derive equations and solutions for linear weights of minimum foreground. In Sec. VI, we present the result of application to the WMAP five year polarization data. In Sec. VII, we make a brief discussion on a few foreground reduction methods with comparisons. In Section VIII, we summarize our investigation with conclusion. In Appendix A, we discuss our unbiased quadratic estimator of power spectrum, which is similar to the WMAP team's cross power estimator, but in more convenient form for use with the HILC implementation.

II. STOKES PARAMETERS

The Stokes parameters describe the state of polarization [16, 17]. For an all-sky analysis, they are measured in reference to $(\hat{e}_\theta, \hat{e}_\phi)$ [1, 4]:

$$\begin{aligned} Q &= \langle E_\theta^2 - E_\phi^2 \rangle, \\ U &= \langle 2E_\theta E_\phi \rangle, \end{aligned}$$

where $\langle \dots \rangle$ indicates average over a period of electromagnetic waves, and \hat{e}_θ and \hat{e}_ϕ are basis vectors of spherical coordinates.

All-sky Stokes parameters are decomposed into spin ± 2 spherical harmonics [4]:

$$Q(\hat{n}) \pm iU(\hat{n}) = \sum_{l,m} a_{\pm 2,lm} \pm 2Y_{lm}(\hat{n}). \quad (1)$$

The spin ± 2 spherical harmonic coefficients $a_{\pm 2,lm}$ are further decomposed into E and B mode [4, 18]:

$$a_{\pm 2,lm} = -(a_{E,lm} \pm i a_{B,lm}), \quad (2)$$

^{*}Electronic address: jkim@nbi.dk

where

$$\begin{aligned} a_{E,lm} &= (-1)^m a_{E,l-m}^*, \\ a_{B,lm} &= (-1)^m a_{B,l-m}^*. \end{aligned}$$

III. FOREGROUND REDUCTION WITH MULTI-FREQUENCY MAPS

Polarization at a frequency ν_k and pixel \mathbf{x} is as follows:

$$\begin{aligned} Q(\mathbf{x}, \nu_k) \pm iU(\mathbf{x}, \nu_k) &= \\ Q_{\text{cmb}}(\mathbf{x}) \pm iU_{\text{cmb}}(\mathbf{x}) + Q_{\text{fg}}(\mathbf{x}, \nu_k) \pm iU_{\text{fg}}(\mathbf{x}, \nu_k) \\ + Q_{\text{noise}}(\mathbf{x}, \nu_k) \pm iU_{\text{noise}}(\mathbf{x}, \nu_k), \end{aligned} \quad (3)$$

where ‘fg’ denote the composite foreground signal. A natural candidate for the estimator of the CMB polarization map is a linear combination of multi-frequency maps, which is as follows:

$$\sum_k w^k(\mathbf{x}) (Q(\mathbf{x}, \nu_k) \pm iU(\mathbf{x}, \nu_k)).$$

To keep the CMB unchanged, a constraint is given such that the sum of linear weights over frequency channels is equal to unity:

$$\sum_k w^k(\mathbf{x}) = 1. \quad (4)$$

With Eq. 3 and 4, it is straightforward to show that

$$\begin{aligned} \sum_k w^k(\mathbf{x}) (Q(\mathbf{x}, \nu_k) \pm iU(\mathbf{x}, \nu_k)) &= \\ Q_{\text{cmb}}(\mathbf{x}) \pm iU_{\text{cmb}}(\mathbf{x}) + \zeta(\mathbf{x}), \end{aligned} \quad (5)$$

where we have neglected noise and

$$\zeta(\mathbf{x}) = \sum_k w^k(\mathbf{x}) (Q_{\text{fg}}(\mathbf{x}, \nu_k) \pm iU_{\text{fg}}(\mathbf{x}, \nu_k)).$$

The variance of the linear combination map is

$$\begin{aligned} \sigma^2 &= \left\langle \left| \sum_k w^k(\mathbf{x}) (Q(\mathbf{x}, \nu_k) \pm iU(\mathbf{x}, \nu_k)) \right|^2 \right\rangle \\ &\approx C^2 + 2 \langle \text{Re} [(Q_{\text{cmb}}(\mathbf{x}) \pm iU_{\text{cmb}}(\mathbf{x})) \zeta(\mathbf{x})] \rangle \\ &\quad + \langle |\zeta(\mathbf{x})|^2 \rangle, \end{aligned} \quad (6)$$

where $\langle \dots \rangle$ denotes average over the whole sky. The term C^2 in Eq. 6 is the variance of CMB polarization signal and is, therefore, independent of linear weights as far as Eq. 4 is satisfied. Since there is no correlation among CMB and foregrounds, we find $\sigma^2 \approx C^2 + \langle |\zeta(\mathbf{x})|^2 \rangle$, and hence a linear combination map of minimum variance contain minimum residual foregrounds. However, the cross terms $\langle \text{Re} [(Q_{\text{cmb}}(\mathbf{x}) \pm iU_{\text{cmb}}(\mathbf{x})) \zeta(\mathbf{x})] \rangle$ is zero only in the limit of infinite number of pixels, which makes

the variance minimization proceed in the way to maximize the cancellation between the residual foreground and CMB [10, 12]. As a part of HILC implementation, we had developed ways to reduce the effect of the cross term (see [13] for details).

The frequency spectrum of real-world foreground vary with positions (see [19] for a recent treatment), and spectral index variation as small as $\sim 10\%$ can have a substantial impact on the linear combination of multi-frequency maps [20]. Therefore, linear weights should possess spatial variability. At the same time, linear weights of minimum foreground are expected to be spatially coherent on small angular scales to a good approximation. Hence, we assume $w^k(\theta, \phi)$ to be some angular functions, which contains spherical harmonics of multipoles up to some cutoff multipole l_{cutoff} . The linear combination map formed with multi-frequency maps

$$\begin{aligned} Q(\theta, \phi) \pm iU(\theta, \phi) &= \\ \sum_i w^k(\theta, \phi) (Q(\theta, \phi, \nu_k) \pm iU(\theta, \phi, \nu_k)), \end{aligned} \quad (7)$$

can be rewritten in spherical harmonic domain, using the Clebsch-Gordon relation:

$$\begin{aligned} a_{\pm 2, LM} &= \\ (-1)^M \sqrt{\frac{2L+1}{4\pi}} \sum_{lm} \sum_{l'm'} \sqrt{(2l+1)(2l'+1)} \\ \times \begin{pmatrix} l & l' & L \\ m & m' & -M \end{pmatrix} \begin{pmatrix} l & l' & L \\ 0 & \pm 2 & \mp 2 \end{pmatrix} \sum_k w_{lm}^k a_{\pm 2, l'm'}^k, \end{aligned} \quad (8)$$

where

$$\begin{aligned} a_{\pm 2, LM} &= \int \pm 2 Y_{LM}^*(\theta, \phi) (Q(\theta, \phi) \pm iU(\theta, \phi)) d\Omega, \\ w_{lm}^k &= \int Y_{lm}^*(\theta, \phi) w^k(\theta, \phi) d\Omega, \\ a_{\pm 2, l'm'}^k &= \int \pm 2 Y_{l'm'}^*(\theta, \phi) (Q(\theta, \phi, \nu_k) \pm iU(\theta, \phi, \nu_k)) d\Omega. \end{aligned}$$

The variance of the linear combination map is equivalently given by

$$\sigma^2 = \sum_{LM} |a_{\pm 2, LM}|^2,$$

where L is bounded by the triangular inequalities:

$$|l - l'| \leq L \leq l + l'. \quad (9)$$

The constraint $\sum_i w^k(\theta, \phi) = 1$ imposed to preserve the CMB signal is expressed in spherical harmonic space as follows:

$$\sum_k w_{00}^k = \sqrt{4\pi}, \quad (10)$$

$$\sum_k w_{lm}^k = 0. \quad (l > 0) \quad (11)$$

IV. DETERMINATION OF LINEAR WEIGHTS

Through variance minimization, we are going to derive equations leading to the linear weights of minimum foreground. Since the function $w^k(\theta, \phi)$ is real-valued, w_{lm}^k obeys the reality condition $w_{l-m}^k = (-1)^m w_{lm}^{k*}$. Therefore, we need to determine only w_{lm}^k ($m \geq 0$). For computational convenience as well as accommodation of the reality condition, we define real-valued spherical harmonic coefficients \tilde{w}_{lm}^k as $\text{Re}[w_{lm}^k]$, $\text{Im}[w_{lm}^k]$ for $m \geq 0$, $m < 0$ respectively. The constraints on \tilde{w}_{lm}^k derived from Eq. 10 and 11 are as follows:

$$\sum_k \tilde{w}_{00}^k = \sqrt{4\pi}, \quad (12)$$

$$\sum_k \tilde{w}_{lm}^k = 0 \quad (l > 0). \quad (13)$$

The linear weights of minimum foreground minimize the variance $\sum_{LM} |a_{\pm 2, LM}|^2$ under the constraints Eq. 12 and 13. The constrained minimization problem is solved conveniently via Lagrange's undetermined multiplier method [11, 21]. With the introduction of Lagrange's multiplier λ_{lm} , it can be shown that the variance is minimized under the constraints Eq. 12 and 13, when

$$\begin{aligned} \frac{\partial \sum_{LM} |a_{\pm 2, LM}|^2}{\partial \tilde{w}_{l'm'}^{k'}} + \lambda_{00} \frac{\partial \left(-\sqrt{4\pi} + \partial \sum_i \tilde{w}_{00}^k \right)}{\partial \tilde{w}_{l'm'}^{k'}} \\ + \sum_{l>0, m} \lambda_{lm} \frac{\partial \sum_i \tilde{w}_{lm}^k}{\partial \tilde{w}_{l'm'}^{k'}} = 0. \end{aligned} \quad (14)$$

By using Eq. 8, it can be shown that Eq. 14 has the following form:

$$\sum_{klm} \left[\alpha_{l'm'lm}^{k'k} \tilde{w}_{lm}^k \right] + \lambda_{l'm'} = 0, \quad (15)$$

where $\alpha_{l'm'lm}^{k'k}$ is

$$\alpha_{l'm'lm}^{k'k} = 2\text{Re} \left[\sum_{LM} \hat{\gamma}_{k'}^*(l', m', L, M) \hat{\gamma}_k(l, m, L, M) \right] \quad (16)$$

and $\hat{\gamma}_k(l_1, m_1, l_3, m_3)$ is

$$\begin{cases} \gamma_k(l_1, m_1, l_3, m_3) + (-1)^{m_1} \gamma_k(l_1, -m_1, l_3, m_3) \\ \gamma_k(l_1, m_1, l_3, m_3) \\ i [\gamma_k(l_1, -m_1, l_3, m_3) - (-1)^{m_1} \gamma_k(l_1, m_1, l_3, m_3)] \end{cases}$$

for $m_1 > 0$, $m_1 = 0$ and $m_1 < 0$ respectively, and

$$\begin{aligned} \gamma_k(l_1, m_1, l_3, m_3) = \\ \sum_{l_2 m_2} (-1)^{m_3} \sqrt{\frac{(2l_1+1)(2l_2+1)(2l_3+1)}{4\pi}} \\ \times \begin{pmatrix} l_1 & l_2 & l_3 \\ m_1 & m_2 & -m_3 \end{pmatrix} \begin{pmatrix} l_1 & l_2 & l_3 \\ 0 & \pm 2 & \mp 2 \end{pmatrix} a_{\pm 2, l_2 m_2}^k. \end{aligned} \quad (17)$$

Therefore, the values of linear weights of minimum foreground can be found in terms of Lagrange's multiplier $\lambda_{l'm'}$ by solving the system of simultaneous linear equations given by Eq. 15. The values of Lagrange's multiplier $\lambda_{l'm'}$ can be easily determined by making the solutions of Eq. 15 satisfy the constraints Eq. 12 and 13. Eq. 12, 13 and 15 can be conveniently put in matrix form. For f frequency channels, Eq. 15 is in matrix notation:

$$\mathbf{A} \cdot \mathbf{w} = -\mathbf{\Pi}^T \mathbf{L}, \quad (18)$$

where

$$\begin{aligned} \mathbf{A}_{j'j} &= \alpha_{l'm'lm}^{k'k}, \\ \mathbf{w}_j &= \tilde{w}_{lm}^k, \\ \mathbf{L}_{j''} &= \lambda_{l'm'}, \end{aligned}$$

for $j' = f(l'^2 + l' + m') + k'$, $j = f(l^2 + l + m) + k$, and $j'' = l'^2 + l' + m'$. \mathbf{A} is a $n \times n$ matrix, and \mathbf{w} and \mathbf{L} are column vectors of length n , and length n/f respectively, where n is the total numbers of \tilde{w}_{lm}^k .

With Eq. 18, \mathbf{w} is solved in terms of n/k undetermined Lagrange multipliers, provided that \mathbf{A} is invertible:

$$\mathbf{w} = -\mathbf{A}^{-1} \mathbf{\Pi}^T \mathbf{L}. \quad (19)$$

The constraints given by Eq. 12 and 13 are:

$$\mathbf{\Pi} \cdot \mathbf{w} = \mathbf{e}. \quad (20)$$

$\mathbf{\Pi}$ is a $\frac{n}{f} \times n$ matrix, given by

$$\Pi_{ij} = \begin{cases} 1 & : f(i-1) + 1 \leq j \leq fi \\ 0 & : \text{otherwise} \end{cases}$$

and \mathbf{e} is a column vector of length n/f , given by

$$\mathbf{e}_j = \begin{cases} \sqrt{4\pi} & : j = 1 \\ 0 & : j > 1 \end{cases}$$

With Eq. 20 and 19, the undetermined n/f Lagrange multipliers are given by:

$$\mathbf{L} = -(\mathbf{\Pi} \mathbf{A}^{-1} \mathbf{\Pi}^T)^{-1} \mathbf{e}, \quad (21)$$

Therefore, linear weights in spherical harmonic space is given as follows:

$$\mathbf{w} = \mathbf{A}^{-1} \mathbf{\Pi}^T (\mathbf{\Pi} \mathbf{A}^{-1} \mathbf{\Pi}^T)^{-1} \mathbf{e}. \quad (22)$$

It should be noted that Eq. 22 is not reduced to $\mathbf{w} = \mathbf{\Pi}^{-1} \mathbf{e}$, since $\mathbf{\Pi}$ and $\mathbf{\Pi}^T$ are not square matrices.

V. FOREGROUNDS REDUCTION FOR E AND B MODE POLARIZATION

Polarization signal of foregrounds as well as CMB can be decomposed into E and B mode, where the E and B mode polarization maps at frequency ν_k are as follows:

$$\begin{aligned} Q_E(\nu_k, \hat{\mathbf{n}}) \pm i U_E(\nu_k, \hat{\mathbf{n}}) &= - \sum_{lm} a_{E, lm}^k \pm 2 Y_{lm}(\hat{\mathbf{n}}), \\ Q_B(\nu_k, \hat{\mathbf{n}}) \pm i U_B(\nu_k, \hat{\mathbf{n}}) &= \mp i \sum_{lm} a_{B, lm}^k \pm 2 Y_{lm}(\hat{\mathbf{n}}). \end{aligned}$$

Foreground sources for E and B mode polarization may have distinct astrophysical origin. Therefore, frequency spectra of foreground of E mode polarization may not be identical with those of B mode polarization. Hence, we assume independent linear weights w_E^k and w_B^k for E and B mode, and find them respectively through minimization of σ_{EE}^2 and σ_{BB}^2 , where

$$\begin{aligned}\sigma_{EE}^2 &= \langle |Q_E(\hat{\mathbf{n}}) \pm iU_E(\hat{\mathbf{n}})|^2 \rangle \\ \sigma_{BB}^2 &= \langle |Q_B(\hat{\mathbf{n}}) \pm iU_B(\hat{\mathbf{n}})|^2 \rangle\end{aligned}$$

For determination of $w_{E,lm}^k$ and $w_{B,lm}^k$, we replace $a_{\pm 2, l_2 m_2}^k$ with $-a_{E, l_2 m_2}^k$ and $\mp i a_{B, l_2 m_2}^k$, respectively, in Eq. 17. After determination of w_E^k and w_B^k , we construct the following maps:

$$\xi(\hat{\mathbf{n}}) = \sum_i w_E^k(\hat{\mathbf{n}}) (Q_E(\hat{\mathbf{n}}, \nu_k) \pm iU_E(\hat{\mathbf{n}}, \nu_k)), \quad (23)$$

$$\beta(\hat{\mathbf{n}}) = \sum_i w_B^k(\hat{\mathbf{n}}) (Q_B(\hat{\mathbf{n}}, \nu_k) \pm iU_B(\hat{\mathbf{n}}, \nu_k)). \quad (24)$$

Using Eq. 4, we may show

$$\begin{aligned}\xi(\hat{\mathbf{n}}) &= Q_E^{\text{cmb}}(\hat{\mathbf{n}}) \pm iU_E^{\text{cmb}}(\hat{\mathbf{n}}) \\ &+ \sum_i w_E^k(\hat{\mathbf{n}}) (Q_E^{\text{fg}}(\hat{\mathbf{n}}, \nu_k) \pm iU_E^{\text{fg}}(\hat{\mathbf{n}}, \nu_k)) \\ &+ \sum_i w_E^k(\hat{\mathbf{n}}) (Q_E^{\text{noise}}(\hat{\mathbf{n}}, \nu_k) \pm iU_E^{\text{noise}}(\hat{\mathbf{n}}, \nu_k)), \\ \beta(\hat{\mathbf{n}}) &= Q_B^{\text{cmb}}(\hat{\mathbf{n}}) \pm iU_B^{\text{cmb}}(\hat{\mathbf{n}}) \\ &+ \sum_i w_B^k(\hat{\mathbf{n}}) (Q_B^{\text{fg}}(\hat{\mathbf{n}}, \nu_k) \pm iU_B^{\text{fg}}(\hat{\mathbf{n}}, \nu_k)) \\ &+ \sum_i w_B^k(\hat{\mathbf{n}}) (Q_B^{\text{noise}}(\hat{\mathbf{n}}, \nu_k) \pm iU_B^{\text{noise}}(\hat{\mathbf{n}}, \nu_k)).\end{aligned}$$

Since the linear weights $w_E^k(\hat{\mathbf{n}})$ and $w_B^k(\hat{\mathbf{n}})$ are spatially varying functions, $\xi(\hat{\mathbf{n}})$ contains B mode polarization of foregrounds and noise, while $\beta(\hat{\mathbf{n}})$ contains E mode polarization of foregrounds and noise. Hence, we filter out B mode polarization from $\xi(\hat{\mathbf{n}})$ and E mode polarization from $\beta(\hat{\mathbf{n}})$. Then, we reconstruct the CMB polarization map as follows:

$$Q(\hat{\mathbf{n}}) \pm iU(\hat{\mathbf{n}}) = \tilde{\xi}(\hat{\mathbf{n}}) + \tilde{\beta}(\hat{\mathbf{n}}), \quad (25)$$

where $\tilde{\xi}(\hat{\mathbf{n}})$ and $\tilde{\beta}(\hat{\mathbf{n}})$ are filtered $\xi(\hat{\mathbf{n}})$ and $\beta(\hat{\mathbf{n}})$ respectively.

VI. APPLICATION TO THE WMAP FIVE YEAR DATA

We have applied our foreground reduction method to the WMAP five year polarization data [8]. Since there exists some anomalous excess power in W band [2, 22], which is not fully understood, we do not use W band data in the reconstruction of CMB polarization maps. We

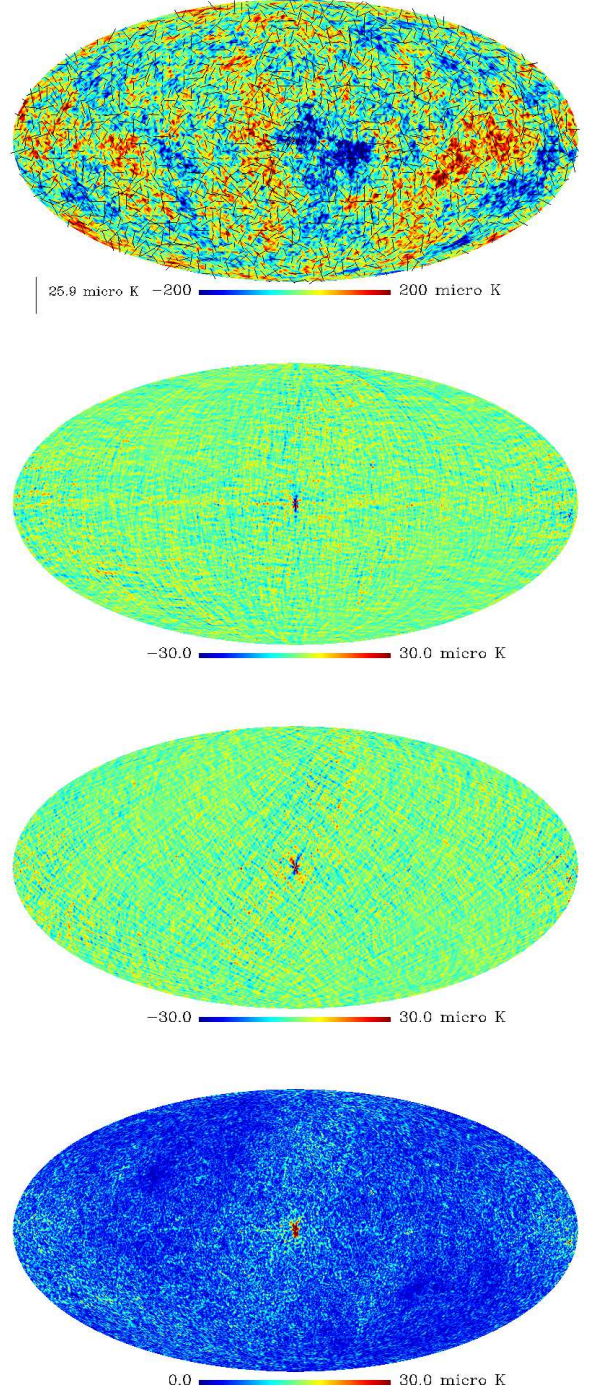


FIG. 1: the 1° FWHM smoothed HILC5YR maps: temperature + polarization, Q, U, and $S = \sqrt{Q^2 + U^2}$ (from top to bottom)

have considered only E mode polarization and obtained E mode spherical harmonic coefficients of band maps as

follows:

$$a_{E,lm}^k = \frac{1}{5} \sum_j a_{E,lm}^{k,j} / B_l^k,$$

where $a_{E,lm}^{k,j}$ are the E mode coefficients of the WMAP j th year single data at k th frequency channel, and B_l^k are the beam transfer functions of the WMAP k th channel [8, 22, 23].

For the frequency channels of multiple differencing assembly (Q and V band), we have used the average value of the multiple differencing assembly data. As discussed in Sec. III, the cross terms in Eq. 6 bias the resulting CMB maps [12]. As a part of HILC method, we had developed methods to reduce the cross term effect (see [13] for details). However, in this work, we do not make special care of the cross term effect, since the cross term effect is negligible, compared to the noise contained in the resulting CMB map.

When linear weights are obtained through variance minimization on noisy data, variance minimization proceeds in the way to minimize noise rather than foregrounds. Since the noise of the WMAP data dominates foreground signal on multipoles higher than ~ 60 , we have used only a_{lm}^k ($l \leq 60$) in variance minimization (i.e. summation over l_2 was done up to 60 in Eq. 17). Though ideally the total number of w_{lm}^k may be as high as the total number of available a_{lm}^k (i.e. the number of parameters may be as many as the number of data), we find that the number of w_{lm}^k , which keeps the matrices in Eq. 22 numerically non-singular, is much smaller than the ideal case (i.e. $l_{\text{cutoff}} \ll 60$). This may be attributed to large bandwidth and relatively small separation of the WMAP frequency channels, because in such configurations the frequency spectrum of foregrounds may not be numerically distinct enough over the channels. Starting with smallest number, we tried various l_{cutoff} and find largest and stable l_{cutoff} for the WMAP polarization data is 5. Therefore, our linear weights $l_{\text{cutoff}} = 5$ is ineffective in cleaning foregrounds, whose frequency spectra vary on the angular scales smaller than $\sim 36^\circ$. However, Fig. 1 shows that our CMB polarization maps do not contain significant foregrounds even inside the region corresponding to the WMAP team's Galactic cut. Besides that, we will be able to set l_{cutoff} as high as coherence angular scales of Galactic foreground frequency spectra, when the polarization data from the upcoming Planck surveyor [24, 25] become available.

As a consequence, linear weights of HILC maps are obtained through minimization of $\sigma^2 = \sum_{L=2,M}^{65} |a_{\pm 2,LM}|^2$ (see Eq. 9). However, these linear weights can be applied to band maps containing higher multipoles. Hence, we used $Q_E(\hat{n}, \nu_k) \pm iU_E(\hat{n}, \nu_k)$ of multipoles ($2 \leq l \leq 700$) in the map reconstruction by Eq. 23 and 25. In Fig. 1 we show the CMB maps 'Harmonic Internal Linear Combination maps' (hereafter, HILC5YR). The top figure in Fig. 1 shows the CMB polarization as headless vectors whose length is proportional to polarization

strength, while the underlying color-coded temperature map is from the HILC5YR temperature map [13]. The second and the third figures show the Stokes parameter Q and U respectively, and the bottom figure shows the polarization strength $S = \sqrt{Q^2 + U^2}$. All figures shown in Fig. 1 have been generated with 1° FWHM beam smoothing to suppress noise for illustrative purpose.

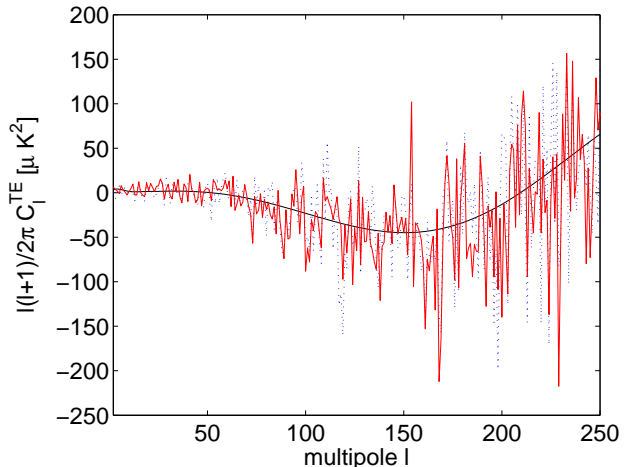


FIG. 2: TE correlation: solid smooth curve (the WMAP best-fit Λ CDM model), solid curve (HILC5YR), dotted curve (WMAP team's estimation)

In Fig. 2, we show our estimation on the TE correlation derived from HILC maps and the estimation by the WMAP team. The theoretical TE correlation of the WMAP best-fit Λ CDM model are shown as a smooth solid curve in the same figure. Since noise in a temperature map and in a polarization map is uncorrelated, we have obtained temperature and E mode correlation by a simple quadratic estimator:

$$C_l^{TE} = (2l+1)^{-1} \sum_m \text{Re} [a_{T,lm} a_{E,lm}^*]. \quad (26)$$

We cannot use a simple quadratic estimator for E mode power spectrum because of a noise bias. Hence we have derived a unbiased quadratic estimator of power spectra, which are similar to the WMAP team's cross power spectra, but in a convenient form to use with HILC method. The details on the unbiased quadratic estimator is given in Appendix A. In Fig. 3, we show the E mode power spectrum obtained from HILC5YR with our estimator. We also show the theoretical E mode power spectrum of the WMAP best-fit Λ CDM model and the WMAP team's estimation [22] in Fig. 3. The large fluctuation in comparison to the theoretical prediction is attributed mostly to the estimation variance associated with noise. Some estimation on E mode power spectra are negative, because they are cross power spectra. From Fig. 2 and 3 we see that the TE correlation and E mode power spectra of HILC5YR are comparable to the WMAP team's estimations and consistent with the

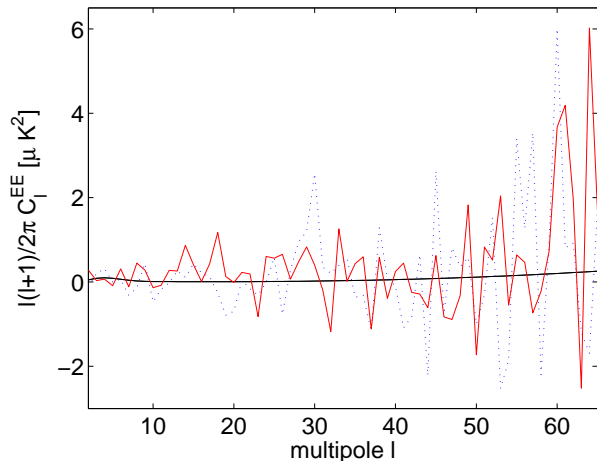


FIG. 3: E mode power spectrum: solid smooth curve(the WMAP best-fit Λ CDM model), solid curve(HILC5YR), dotted curve (WMAP team's power spectra)

WMAP best-fit Λ CDM model. The linear weights of HILC5YR, which are continuous over the entire sky, are shown in Fig. 4. It is worth to note that the linear weights for Q and V bands are positive over the entire sky. We have computed the variance of our linear weights by $w_l^k = (2l+1)^{-1} \sum_m |w_{lm}^k|^2$ to quantify the spatial variation of our linear weights on different angular scales. Fig. 5 shows that w_l^k tends to decrease with increasing multipole with w_0^k being the highest.

VII. COMPARISON WITH OTHER METHODS

We restrict our discussion to the methods of currently available CMB polarization maps. Before proceeding to comparison, we would like to reiterate that the major goal of HILC approach is to reconstruct a whole-sky CMB map, which is important for the study of CMB polarization on large scales.

The merits of HILC approach is that it incorporates spatial variability of foreground frequency spectrum in a natural way, and barely rely on external information on foregrounds. Its major limitation is poor performance for low Signal-to-noise ratio (SNR) data.

The WMAP team produced foreground reduced maps by template fitting method, whose model templates are derived from K band of the WMAP data, and Finkbeiner dust model 8 [26]. Meanwhile, there is strong arguments against the interpretation of K band as synchrotron templates [27, 28] and it turns out that the template models are not sufficient to make a good fits inside and outside the Galactic cut at the same time. As a consequence, there is heavy foreground contamination inside the Galactic cut, which makes the template-fitted methods unsuitable for a whole sky map.

The WMAP team also produced a low resolution

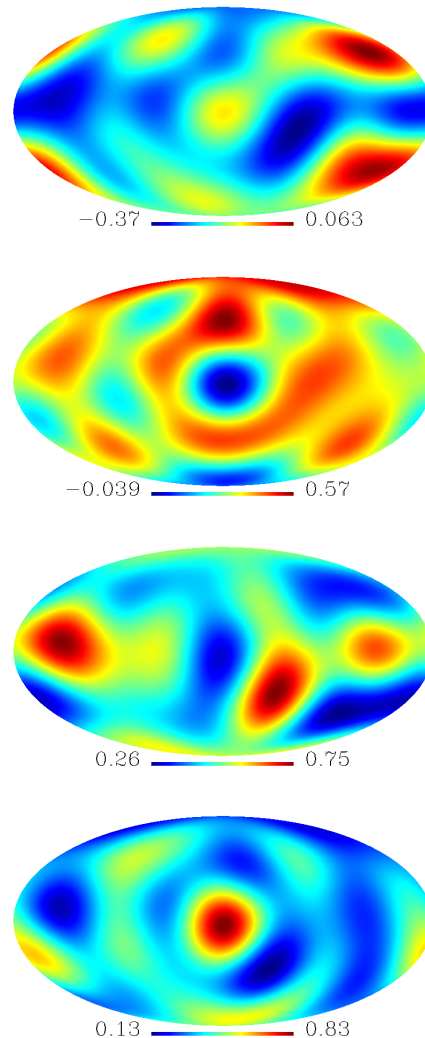


FIG. 4: The HILC5YR linear weight for K, Ka, Q, and V band (from top to bottom)

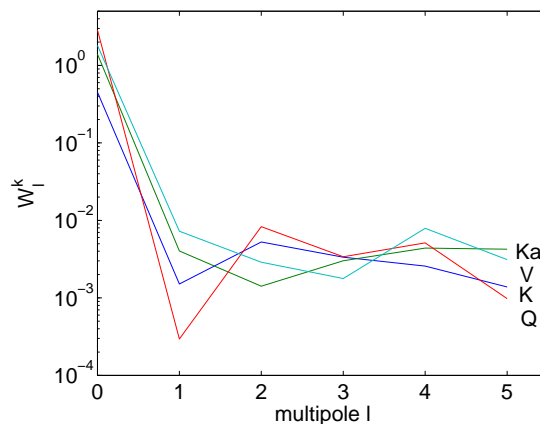


FIG. 5: Variance of the HILC5YR linear weights

CMB polarization map by Markov Chain Monte Carlo (MCMC) method [9]. The merits of this approach is that it utilizes external information on polarized foreground as a priori. Besides low resolution, its major limitation is that it does not work well within Galactic cut [9] and therefore not suitable for a whole-sky map.

VIII. DISCUSSION

Using the WMAP 5 year polarization data, we have reconstructed whole-sky CMB polarization maps through Harmonic Linear Combination method. From our CMB polarization maps without any masking, we have obtained TE correlation and E mode power spectrum, which are similar to the WMAP team's estimation.

Because of the low SNR of the WMAP polarization data, our HILC polarization maps contain relatively significant noise. Besides that, low SNR of multi-frequency data seriously degrades foreground reduction of our method, which are relevant to all variants of ILC method. Therefore, we should warn that our CMB polarization maps should be used with some caution. However, the major aims of this work are to demonstrate HILC on polarization data in preparation for the future Planck data and to reconstruct whole-sky CMB polarizations maps, whose power spectra are similar to the WMAP team's estimation.

HILC method is, in general, ineffective in cleaning point sources in comparison to diffuse Galactic foregrounds because of assumed finite l_{cutoff} . However, we can effectively suppress point-source contamination by applying point-source filter derived by [29] at the post-HILC stage.

In comparison to other foreground cleaning method (e.g. template fitting methods), the effectiveness of our method improves sharply with increase in Signal-to-noise ratio (SNR), frequency channels and angular resolution of the observation. Hence, our method will allow us to reduce foregrounds effectively in the polarization data from the upcoming Planck surveyor [24, 25].

The CMB polarization map, estimated power spectra and linear weights are available from <http://www.nbi.dk/~jkim/hilc>.

IX. ACKNOWLEDGMENTS

We acknowledge the use of the Legacy Archive for Microwave Background Data Analysis (LAMBDA). Some of the results in this paper have been derived using the HEALPix [30, 31] package. This work is supported by FNU grant 272-06-0417, 272-07-0528 and 21-04-0355.

APPENDIX A: UNBIASED QUADRATIC ESTIMATOR OF POWER SPECTRA

The estimator derived here is equally applicable to temperature, E mode and B mode power spectrum respectively. Since spherical harmonic coefficients of single-year maps consist of signal and noise terms:

$$a_{lm}^{k,j} = S_{lm}^k + N_{lm}^{k,j}, \quad (\text{A1})$$

spherical harmonic coefficients of band maps, constructed by averaging n single-year maps, is as follows:

$$\begin{aligned} a_{lm}^k &= \frac{1}{n} \sum_j a_{E,lm}^{k,j}, \\ &= S_{lm}^k + \frac{1}{n} \sum_j N_{lm}^{k,j}, \end{aligned}$$

where S_{lm}^k denote signal of k th frequency channel and $N_{lm}^{k,j}$ denotes noise of j th year data at k th frequency channel. Given the linear weights w_{lm}^k yielding minimum residual foreground, the spherical harmonic coefficient a_{lm} of a HILC map is as follows:

$$a_{lm} = \sum_k w_{lm}^k \otimes S_{lm}^k + \frac{1}{n} \sum_k \sum_j w_{lm}^k \otimes N_{lm}^{k,j}, \quad (\text{A2})$$

where \otimes denotes spherical harmonic convolution given by Clebsch-Gordon relation.

Spherical harmonic coefficients of a HILC map may be split into signal and noise terms:

$$a_{lm} = S_{lm} + \frac{1}{n} \sum_j N_{lm}^j.$$

where $S_{lm} = \sum_k w_{lm}^k \otimes S_{lm}^k$ and $N_{lm}^j = \sum_i w_{lm}^i \otimes N_{lm}^{i,j}$. A simple quadratic estimator for power spectrum gives

$$\begin{aligned} &(2l+1)^{-1} \sum_m |a_{lm}|^2 \\ &= (2l+1)^{-1} \left(\sum_m |S_{lm}|^2 + \frac{1}{n^2} \sum_m \sum_j |N_{lm}^j|^2 \right. \\ &\quad + \frac{1}{n} \sum_m \sum_j S_{lm} N_{lm}^{j*} + S_{lm}^* N_{lm}^j \\ &\quad \left. + \frac{1}{n^2} \sum_m \sum_{j>j'} N_{lm}^j N_{lm}^{j'*} + N_{lm}^{j*} N_{lm}^{j'} \right) \end{aligned} \quad (\text{A3})$$

where the summation is over $1 \leq j' \leq n$ and $j' < j \leq n$. As seen from Eq. A3, the term $|N_{lm}^j|^2$ is always positive, and hence makes Eq. A3 biased.

Now, consider the following quadratic estimator, which has an extra term:

$$\hat{C}_l = (2l+1)^{-1} \left(\sum_m |a_{lm}|^2 - \frac{1}{n^2(n-1)} \sum_m \sum_{j>j'} |a_{lm}^j - a_{lm}^{j'}|^2 \right) \quad (\text{A4})$$

where

$$a_{lm}^j = \sum_k w_{lm}^k \otimes a_{lm}^{k,j}, \quad a_{lm}^{j'} = \sum_k w_{lm}^k \otimes a_{lm}^{k,j'}.$$

Using Eq. A1, A3 and A4, we show that

$$\begin{aligned} \hat{C}_l = & (2l+1)^{-1} \left(\sum_m |S_{lm}|^2 + \frac{1}{n} \sum_m \sum_j S_{lm} N_{lm}^{j*} + S_{lm}^* N_{lm}^j \right. \\ & \left. + \frac{1}{n(n-1)} \sum_m \sum_{j>j'} N_{lm}^j N_{lm}^{j'*} + N_{lm}^{j*} N_{lm}^{j'} \right) \end{aligned} \quad (\text{A5})$$

Since the expectation value of \hat{C}_l is

$$\langle \hat{C}_l \rangle = (2l+1)^{-1} \left\langle \sum_m |S_{lm}|^2 \right\rangle,$$

we find \hat{C}_l unbiased. Now, let us consider the variance of the estimator \hat{C}_l . We neglect residual foreground in signal S_{lm} , assuming foreground reduction is very effective. Since $\sum_m |S_{lm}|^2 / C_l$ follows Chi-Squared distribution of $2l+1$ degrees of freedom, the variance of the first term on the right hand side of Eq. A5 is

$$\langle |\sum_m |S_{lm}|^2|^2 \rangle = 2(2l+1)(C_l)^2. \quad (\text{A6})$$

Taking into the reality conditions $S_{lm} = (-1)^l S_{l-m}^*$ and $N_{lm}^j = (-1)^l N_{l-m}^{j*}$, we find the variance of the second term and the third term on the right hand side of Eq. A5 are respectively:

$$\langle |\sum_m \sum_j S_{lm} N_{lm}^{j*} + S_{lm}^* N_{lm}^j|^2 \rangle = (2l+1) \cdot n \cdot 4 \cdot C_l N_l, \quad (\text{A7})$$

and

$$\begin{aligned} & \langle |\sum_m \sum_{j>j'} N_{lm}^j N_{lm}^{j'*} + N_{lm}^{j*} N_{lm}^{j'}|^2 \rangle \\ & = (2l+1) \cdot \frac{n(n-1)}{2} \cdot 4 \cdot (N_l)^2, \end{aligned} \quad (\text{A8})$$

where C_l and N_l are theoretical power spectrum of CMB and noise respectively. In deriving Eq. A7 and A8, we have made the approximation $\langle N_{lm}^{j*} N_{lm}^{j'} \rangle \propto \delta_{mm'}$, which is not true in real observations because of anisotropic noise. Hence our estimation on the variance of \hat{C}_l will be underestimated in real observations. Noting there is no correlation among the first, the second, and the third terms on the the right hand side of Eq. A5, we may show that the estimation variance of \hat{C}_l is

$$(\Delta \hat{C}_l)^2 = \frac{2}{2l+1} ((C_l)^2 + \frac{2}{n} C_l N_l + \frac{1}{n(n-1)} (N_l)^2).$$

We can also obtain the same result with \hat{C}_l by applying the WMAP team's cross-power estimator to a pair of distinct single-year maps and averaging estimation over all combinations. However, \hat{C}_l by Eq. A4 is more convenient for HILC implementation.

-
- [1] Marc Kamionkowski, Arthur Kosowsky, and Albert Stebbins. Statistics of cosmic microwave background polarization. *Phys. Rev. D*, 55:7368, 1997.
 - [2] L. Page and et al. Three year wilkinson microwave anisotropy probe (WMAP) observations: Polarization analysis. *Astrophys.J.Suppl.*, 170:335, 2007. astro-ph/0603450.
 - [3] Uros Seljak and Matias Zaldarriaga. Signature of gravity waves in polarization of the microwave background. *Phys. Rev. Lett.*, 78:2054, 1997.
 - [4] M. Zaldarriaga and U. Seljak. An all-sky analysis of polarization in the microwave background. *Phys. Rev. D*, 55:1830, 1997.
 - [5] Max Tegmark, Daniel J. Eisenstein, Wayne Hu, and Angelica de Oliveira-Costa. Foregrounds and forecasts

- for the cosmic microwave background. *Astrophys. J.*, 530:133, 2000.
- [6] Anglica de Oliveira-Costa, Max Tegmark, Christopher O'dell, Brian Keating, Peter Timbie, Efstathiou George, and George Smoot. The large-scale polarization of the microwave foreground. *New Astronomy Reviews*, 47:1117, 2003.
- [7] M. Tegmark and G. Efstathiou. A method for subtracting foregrounds from multi-frequency CMB sky maps. *Mon. Not. R. Astron. Soc.*, 281:1297, 1996.
- [8] G. Hinshaw and et al. Five-year wilkinson microwave anisotropy probe (WMAP) observations: Data processing, sky maps, and basic results. 2008. arXiv:0803.0732.
- [9] B. Gold and et al. Five-year wilkinson microwave anisotropy probe (WMAP) observations: Galactic

- foreground emission. *submitted to ApJS*, 2008. arXiv:0803.0715.
- [10] J. Delabrouille, J.-F. Cardoso, M. Le Jeune, M. Betoule, G. Fay, and F. Guillaux. A full sky, low foreground, high resolution CMB map from WMAP. *submitted to AA*, 2008. arXiv:0807.0773.
 - [11] H. K. Eriksen, A. J. Banday, K. M. Gorski, and P. B. Lilje. On foreground removal from the Wilkinson Microwave Anisotropy Probe data by an Internal Linear Combination method: Limitations and implications. *Astrophys. J.*, 612:633, 2004.
 - [12] G. Hinshaw and et al. Three-year Wilkinson Microwave Anisotropy Probe (WMAP) observations: Temperature analysis. *Astrophys. J. Suppl.*, 170:288, 2007.
 - [13] Jaiseung Kim, Pavel Naselsky, and Per Rex Christensen. A CMB map derived from the WMAP data through harmonic linear combination. *Phys. Rev. D*, 375:625, 2007. <http://www.nbi.dk/~jkim/hilc>.
 - [14] Chan-Gyung Park, Changbom Park, and J. Richard Gott III. Cleaned three-year wmap cmb map: Magnitude of the quadrupole and alignment of large scale modes. *Astrophys. J.*, 660:959, 2007.
 - [15] Max Tegmark, Angelica de Oliveira-Costa, and Andrew Hamilton. A high resolution foreground cleaned CMB map from WMAP. *Phys. Rev. D*, 68:123523, 2003.
 - [16] J. Kraus. *Radio Astronomy*. Cygnus-Quasar Books, Powell, Ohio USA, 2nd edition, 1986.
 - [17] K. Rohlfs and T. L. Wilson. *Tools of Radio Astronomy*. Springer-Verlag, New York, NY USA, 4th edition, 2003.
 - [18] M. Zaldarriaga. CMB polarization experiments. *Astrophys. J.*, 503:1, 1998.
 - [19] R. D. Davies, C. Dickinson, A.J. Banday, T. R. Jaffe, and K. M. Gorski. A determination of the spectra of galactic components observed by wmap. *Mon. Not. R. Astron. Soc.*, 370:1125, 2006.
 - [20] Max Tegmark. Removing real-world foregrounds from cmb maps. *Astrophys. J.*, 502:1, 1998.
 - [21] George B. Arfken and Hans J. Weber. *Mathematical Methods for Physicists*. Academic Press, San Diego, CA USA, 5th edition, 2000.
 - [22] M. R. Nolte and et al. Five-year Wilkinson Microwave Anisotropy probe (WMAP) observations: Angular power spectra. *submitted to ApJS*, 2008. arXiv:0803.0593.
 - [23] R. S. Hill and et al. Five-Year Wilkinson Microwave Anisotropy Probe (WMAP) observations: Beam maps and window functions. *submitted to ApJS*, 2008. arXiv:0803.0570.
 - [24] J. Clavel and J. A. Tauber. The Planck mission. volume 15 of *EAS Publications Series*, page 395, 2005.
 - [25] J. A. Tauber. The Planck mission: Overview and current status. *Astrophysical Letters and Communications*, 37:145, 2000.
 - [26] Douglas P. Finkbeiner, Marc Davis, and David J. Schlegel. Extrapolation of galactic dust emission at 100 microns to CMBR frequencies using FIRAS. *Astrophys. J.*, 524:867, 1999.
 - [27] Angelica de Oliveira-Costa, Max Tegmark, R.D. Davies, Carlos M. Gutierrez, A.N. Lasenby, R. Rebolo, and R.A. Watson. The quest for microwave foreground x. *Astrophys. J.*, 606:L89, 2004.
 - [28] Douglas P. Finkbeiner, Glen I. Langston, and Anthony H. Minter. Microwave interstellar medium emission in the green bank galactic plane survey: Evidence for spinning dust. *Astrophys. J.*, 617:350, 2004.
 - [29] Max Tegmark and Angelica de Oliveira-Costa. Removing point sources from cmb maps. *Astrophys. J.*, 500:L83, 1998.
 - [30] K. M. Gorski, E. Hivon, A. J. Banday, B. D. Wandelt, F. K. Hansen, M. Reinecke, and M. Bartelman. HEALPix – a framework for high resolution discretization, and fast analysis of data distributed on the sphere. *Astrophys. J.*, 622:759, 2005. <http://healpix.jpl.nasa.gov>.
 - [31] K. M. Gorski, B. D. Wandelt, F. K. Hansen, E. Hivon, and A. J. Banday. The HEALPix primer. *astro-ph/9905275*, 1999.